Cite this article
Louw H, Kearsley E and Jacobsz SW (2022)
Modelling horizontally loaded reinforced-concrete piles in a geotechnical centrifuge.
International Journal of Physical Modelling in Geotechnics **22(1)**: 14–25,
https://doi.org/10.1680/jphmg.20.00016

Research Article
Paper 2000016
Received 13/02/2020;
Accepted 27/10/2020;
Published online 15/12/2020

Keywords: centrifuge modelling/piles & piling/soil/structure interaction

International Journal of Physical Modelling in Geotechnics

ice Publishing

Modelling horizontally loaded reinforced-concrete piles in a geotechnical centrifuge

1 **Hendrik Louw** MEng (Pret)
Graduate student, Department of Civil Engineering, University of Pretoria, Pretoria, South Africa (Orcid:0000-0002-0686-7364) (corresponding author: henilouw@gmail.com)

2 **Elsabe Kearsley** PhD (Leeds)
Professor, Department of Civil Engineering, University of Pretoria, Pretoria, South Africa (Orcid:0000-0003-0458-8908)

3 **Schalk Willem Jacobsz** PhD (Cantab)
Professor, Department of Civil Engineering, University of Pretoria, Pretoria, South Africa (Orcid:0000-0002-7439-2276)



The design of pile foundations to accommodate horizontal loads is a complex soil–structure interaction problem. Current small-scale laboratory testing of pile foundations is mostly focused on metal piles, which raises the question of the validity of results from these tests, and the principles derived, for the use of analysing and designing reinforced-concrete piles, where not only the soil, but also the piles exhibit highly non-linear material behaviour. This paper describes centrifuge tests that were conducted on scaled aluminium and reinforced-concrete single piles, subjected to lateral loading, with the aim of establishing the suitability of using aluminium alloys for modelling scaled reinforced-concrete piles. With responses similar to literature, both pile types proved to model the behaviour of laterally loaded piles well as far as bending and deflection at low loads are concerned. At larger loads, the reinforced-concrete pile cracked, resulting in non-linear material response, which contributed significantly to the difference in the behaviour between the piles studied. It was observed that the behaviour of reinforced-concrete piles under serviceability loads would not be captured using materials that cannot replicate the reduction in stiffness resulting from crack formation in concrete.

Notation

A_m	cross-sectional area of the model pile
D_m	outside diameter of the model pile
EI_A	flexural stiffness of the aluminium model pile
EI_C	flexural stiffness of the reinforced-concrete model pile
E_m	stiffness of the model pile
e_L	load eccentricity from the soil surface
H	lateral load
H_{crack}	lateral load causing cracking of the pile
H_u	ultimate lateral capacity of the pile
I_m	second moment of area of the model pile
K_N	absolute pile stiffness after N cycles
K_p	passive earth pressure coefficient
k_N	secant pile stiffness after N cycles
L_m	embedment length of the model pile
M	bending moment
M_{crack}	cracking bending moment of the pile
M_{max}	maximum bending moment in the pile
M_{per}	permanent bending moment
M_{yield}	yielding bending moment of the pile
N	number of load cycles
n	centrifuge scaling factor
t_m	wall thickness of the model pile
y_h	maximum pile head displacement
y_{hper}	permanent pile head displacement
y_{hpgain}	permanent pile head displacement gain
z_s	depth below the soil surface
γ	unit weight of the soil
σ_{yield}	yield stress of the pile

1. Introduction

With full-scale field testing being expensive and challenging to undertake, small-scale models have been widely used in civil engineering practice to improve the understanding of the behaviour of complex engineering problems. By combining

both small-scale structural (Noor and Boswell, 1992; Sabnis *et al.*, 1983) and soil modelling (Schofield, 1980) in a centrifuge, complex soil–structure interaction problems can be investigated, as the centrifugal forces ensure that realistic soil stresses and strains are generated, despite the small size of the models. Reinforced-concrete structures have typically been modelled in the centrifuge using aluminium alloys, due to the ease of machining and fabricating these elements, as opposed to actual concrete that is difficult to scale, as has been indicated by Sabnis *et al.* (1983) as well as Noor and Boswell (1992). Madabhushi (2015) indicated that, although the axial and bending behaviour of structural components are captured by using these alloys, the failure mechanism is not, as the yield stress and stiffness of the materials differ. Reinforced-concrete elements are designed to crack in tension under service loads, so that the flexural stiffness of elements decreases with increasing loading, thus complicating the behaviour of concrete elements. It is therefore important to use appropriate materials to model the behaviour of structural members when studying soil–structure interaction problems.

The design of pile foundations to accommodate horizontal loads is primarily based on either the ultimate lateral resistance of the pile or soil, or the load–deflection response of the soil–pile system. As indicated by Poulos and Davis (1980) as well as Poulos and Hull (1989), the behaviour of these foundations represents a complex soil–structure interaction problem concerned with the relative stiffness between the pile and the surrounding soil. A large number of full-scale tests have been conducted in the past to evaluate the response of laterally loaded pile foundations subjected to both monotonic and cyclic lateral loading conditions, referring for example to Reese *et al.* (1974), Brown *et al.* (1987), Little and Briaud (1988) and Li *et al.* (2015, 2017). In addition, scale model piles, typically fabricated from aluminium, have been tested at 1***g*** or at an accelerated ***g***-level in a geotechnical centrifuge (Abadie and Byrne, 2014; Dyson and Randolph, 2001; Georgiadis *et al.*, 1992; Kirkwood and Haigh, 2014; Leblanc *et al.*, 2010; Li *et al.*, 2010; Lin *et al.*, 2015; Yan and Byrne, 1992; Zhu *et al.*, 2016). Most design recommendations stemming from full-scale and scaled tests are based on the observed responses of mostly metal piles. Limited research has been published on the behaviour of horizontally loaded reinforced-concrete piles (Little and Briaud, 1988; Nip and Ng, 2005; Noor and Boswell, 1992; Ruesta and Townsend, 1997). Due to the elastic behaviour of metal sections, these tests typically focused on the soil component of the soil–structure interaction problem, allowing for non-linear behaviour of the soil surrounding the pile on load application, mostly disregarding the possible non-elastic behaviour of the pile itself. Considering the low tensile capacity of concrete (approximately 10% of its compressive strength), Mosley *et al.* (2012) mentioned that nearly all reinforced-concrete structures are designed with the assumption that the concrete does not resist any tensile forces and thus the structures are assumed to be cracked. This raises questions about the validity of using metal piles to model the behaviour of reinforced-concrete piles.

Monotonic behaviour of single piles has been discussed by a number of researchers for both full-scale and scaled models (Brown *et al.*, 1987; Dyson and Randolph, 2001; Georgiadis *et al.*, 1992; Li *et al.*, 2017; Lin *et al.*, 2015; Verdure *et al.*, 2003; Zhu *et al.*, 2016). However, the application of pure monotonic lateral loading is rarely encountered in practice, with cyclic lateral loading being more typical of real-life live loading seen in practice. The response to cyclic loading can be predicted from the monotonic response by applying degradation factors (Long and Vanneste, 1994). Additionally, many researchers have indicated that, under long-term cyclic loading of the soil–pile system, soil around the pile densified rather than degraded (Leblanc *et al.*, 2010). When considering the perceived increase in stiffness (densifying) of the soil–pile system with cyclic lateral loading, Abadie and Byrne (2014) indicated that, based on work from Little and Briaud (1988), the term stiffness should be carefully considered and explained. They classified the stiffness in one of two ways. The first is defined as the absolute pile stiffness (K_N), which relates the soil state at cycle N to the initial state and describes the evolution of the interaction between the pile and the surrounding soil. The second is defined as the secant pile stiffness (k_N), which characterises the state of the soil–pile interaction after N cycles. This evolution in stiffness is critical and, for example, influences the change in natural frequency of the structure with cycle number. The concept of secant pile stiffness has been extensively used by many researchers (Leblanc *et al.*, 2010; Li *et al.*, 2010; Verdure *et al.*, 2003) for explaining the behaviour of soil under cyclic loading. They observed densification of the soil in front of piles due to repetitive loading, with Li *et al.* (2015) suggesting that the subsequent increase in stiffness caused by cyclic loading is related to particle and principle stress re-orientation.

Besides bending moments that develop in piles due to applied cyclic lateral loading, Kirkwood and Haigh (2014) mentioned the occurrence of locked-in (permanent) moments or stresses in piles after load removal. This was attributed to the repetitive loading of the piles, changing the soil conditions surrounding the piles, thus causing stresses in the soil and, in turn, locked-in moments, which increased with the number of load cycles applied.

Werkmeister *et al.* (2001) investigated the effect of cyclic loading on the performance of unbound granular materials using cyclic triaxial tests. They referred to the concept of 'shakedown' associated with the repetitive loading as originally proposed by Johnson (1986). The shakedown concept and

associated permanent strain accumulation can be described by three ranges (Werkmeister *et al.*, 2001).

- Range A – plastic shakedown, where under low applied stress the soil responds plastically for a finite number of load applications and eventually becomes entirely resilient after a 'post-compaction' period, with no further permanent strains occurring after that.
- Range B – intermediate response amounts to plastic creep.
- Range C – incremental collapse, where continuing incremental plastic deformation was observed for each additional load cycle. Therefore, at higher load levels the response was always plastic, and each load application resulted in a progressive increment of permanent strain at the same load level.

In this research study, tests were conducted on scaled aluminium and reinforced-concrete single piles, subjected to both monotonic and cyclic lateral loading in a geotechnical centrifuge. The purpose of this study was to determine whether aluminium sections in a centrifuge could be used to realistically model the monotonic and cyclic response of reinforced-concrete piles subjected to lateral loading. Tests were thus conducted to establish and compare the response of laterally loaded scaled aluminium piles to that of reinforced-concrete piles under monotonic and cyclic loading conditions.

2. Experimental set-up

Centrifuge models were designed and constructed using both a scaled aluminium pile and a reinforced-concrete pile. Lateral load was applied at the pile head at 30***g***, during which the behaviour of the two piles was observed and compared. Both monotonic and cyclic behaviour were studied, taking into account the effect of an uncracked against cracked reinforced-concrete pile in dry sand.

2.1 Model pile design

The model pile dimensions were selected to represent a 600 mm full-scale reinforced-concrete pile (Byrne and Berry, 2008), containing $6 \times$ Y20 main reinforcing bars. As the primary problem concerned bending of the piles, the flexural rigidity (E_mI_m) of both the scaled aluminium and reinforced-concrete piles were scaled, using the appropriate scaling laws (Schofield, 1980), to represent the above-mentioned pile. An embedment length of 10.5 m was selected, which corresponded to 350 mm at model scale. Both piles had a total length of 400 mm, with 350 mm embedded in the soil. For the scaled aluminium model pile, a standard hollow aluminium tube was used with dimensions as indicated in Table 1. The modulus of elasticity of aluminium was assumed as 70 GPa. In Table 1, D_m refers to the external pile diameter, t_m to the wall thickness, A_m to the pile's cross-sectional area and I_m to the second moment of area of the pile cross-section.

Table 1. Scaled aluminium and reinforced-concrete pile dimensions

Pile type	D_m: mm	t_m: mm	A_m: mm^2	I_m: mm^4
Aluminium	19.2	1.3	73.1	2943
Reinforced concrete	21.1	—	352.9	10 036

Table 2. Scaled concrete mix composition

Material	Relative density	kg/m^3
Cement (CEM V/A (S-V) 42.5N)	2.78	300
Water	1.00	250
Dolomite crusher sand	2.85	1870
Superplasticiser	1.06	21

Table 3. Scaled concrete strengths and stiffnesses

Property	Specimen size	28 day
Compression strength: MPa	50 mm cube	35.8
Splitting cylinder strength: MPa	50 mm cylinder (100 mm long)	2.8
Secant modulus of elasticity: GPa	50 mm cylinder (100 mm long)	20.5

The scaled reinforced-concrete pile was cast from concrete with a characteristic compressive strength of 25 MPa. The concrete mix design was scaled down as indicated in Table 2. Dolomite crusher sand, passing the 1 mm sieve size, was selected for both the fine and coarse aggregate, which is representative of a typical 26 mm dolomite stone, scaled down. Superplasticiser was added to the mix to increase workability. Based on trial mix results, the dimensions of the reinforced-concrete pile were determined as indicated in Table 1, with a small difference observed between the two pile diameters (aluminium and reinforced concrete). It should also be noted that the cross-section and second moment of area values indicated for the reinforced-concrete pile is for an uncracked concrete section. For modelling the main reinforcing bars, 6×0.60 mm stainless-steel wires were used, confined by a 0.21 mm stainless-steel wire spiral with a pitch of approximately 10 mm and diameter of 17 mm. To ensure sufficient bond between the steel wire and the concrete, the steel wire was soaked in hydrochloric acid prior to cage construction.

The material properties of the scaled-down concrete – that is, the compressive strength, splitting tensile strength, as well as the secant modulus of elasticity was measured after 28 days and are reported in Table 3 (values represent averages of sets of three measured values). Small test specimens were cast to assess whether the strength of the scaled concrete was representative (Noor and Boswell, 1992). The specimens tested were cured together with the concrete piles to ensure that the measured

material properties were representative of that of the pile. The density of the scaled concrete was determined as 2382 kg/m^3.

2.2 Centrifuge testing procedures

Tests were conducted using the geotechnical centrifuge at the University of Pretoria (Jacobsz *et al.*, 2014). The typical model set-up is illustrated in Figure 1. An aluminium strongbox was used with a wall thickness of 50 mm, 400 mm wide on the internal side, 600 mm long and 400 mm deep. Piles were located in the centre of the strongbox, with a compressive horizontal load applied to the pile heads using a linear actuator. A load cell was attached to the front of the actuator shaft. The load was applied to the piles through an aluminium pile cap that was fixed to the pile head.

The horizontal movement and rotation of the pile caps were measured above the soil surface using a series of linear variable differential transducers (LVDTs) fixed to an aluminium frame mounted to the strongbox. For subsurface horizontal pile movement, a bending beam displacement transducer was used that was placed inside the strongbox.

To measure the strain development and corresponding bending response of the piles, both the aluminium and reinforced-concrete piles were instrumented with 12 120 Ω precision resistance strain gauges. Figure 2 indicates the placement of the strain gauges along the length of the pile. These strain gauges were attached to both sides of each pile, connected in 12 quarter-Wheatstone bridges to obtain independent strain measurements. As the maximum bending moment was expected to occur between four and five pile diameters below the soil surface (Georgiadis *et al.*, 1992; Zhu *et al.*, 2016), instrumentation was concentrated in this area.

The surface roughness has a significant effect on the load–deflection and bending moment distribution of laterally loaded piles (Taylor, 1995). Fine silica sand was glued to the outside of both piles along the entire embedment length as shown in Figure 2. This allowed both piles to have the same surface roughness and therefore similar soil–pile interaction properties. The thickness of the silica sand layer on both piles were similar, adding an additional 0.5–1 mm to the outer pile diameter. The sand layer was assumed not to contribute to the bending stiffness of the piles.

Both piles were calibrated in bending in the laboratory before the centrifuge tests were conducted. The calibration revealed a difference in the flexural rigidity of the two piles which had to be taken into account when comparing test results.

All centrifuge tests were carried out using a fine silica sand with a mean particle size of 138 μm and a specific gravity of

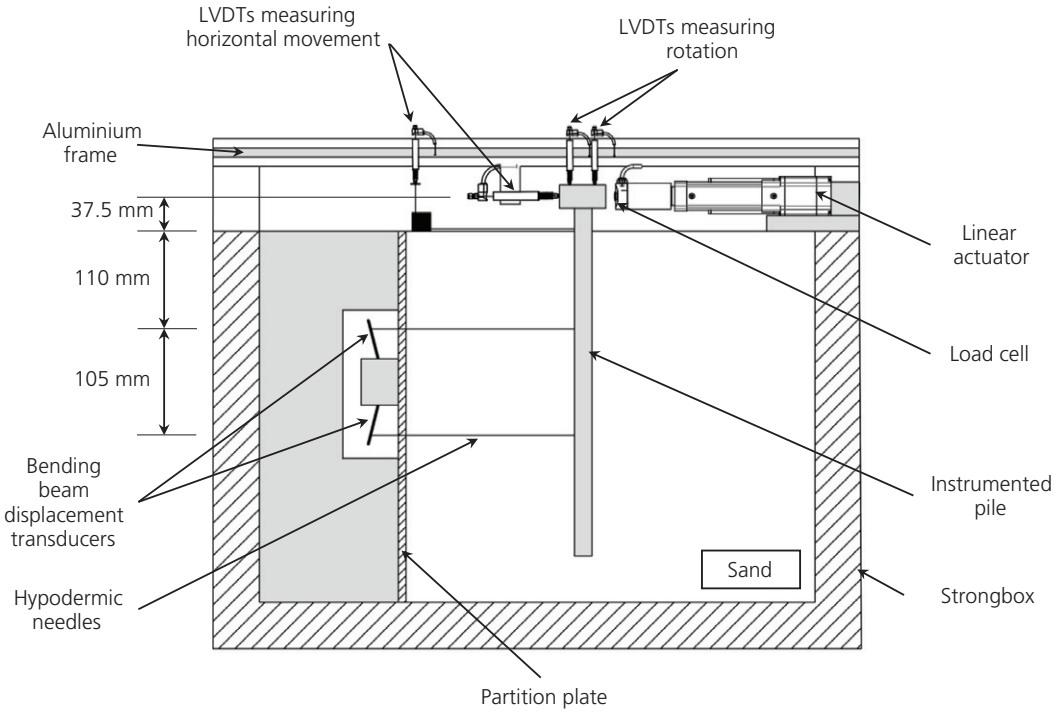

Figure 1. Model set-up

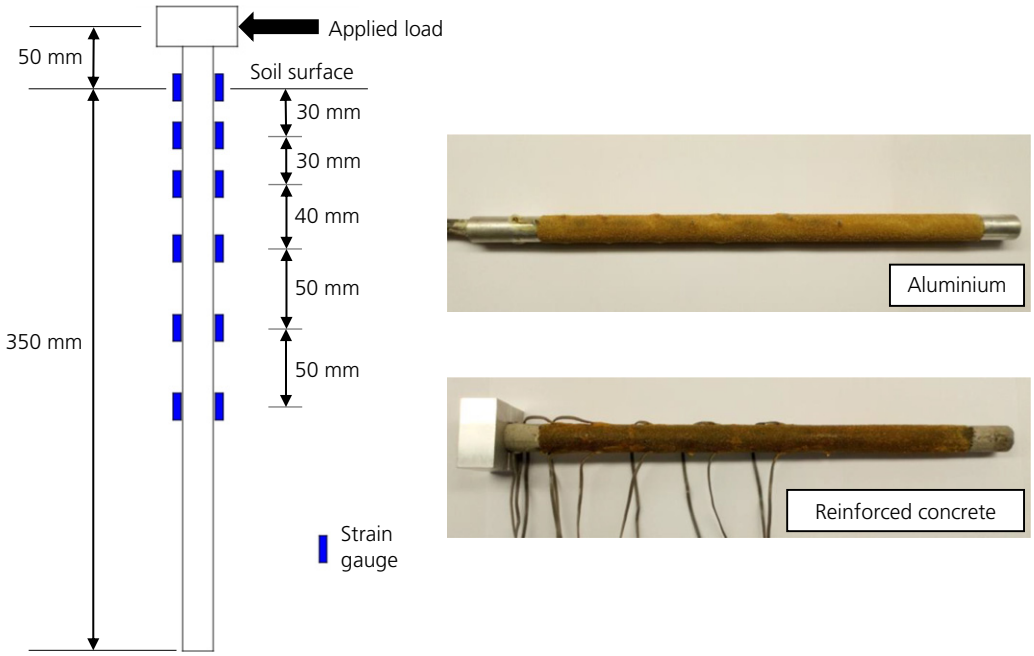

Figure 2. Strain gauge placement on piles and instrumented model piles

Table 4. Ultimate horizontal load and bending moment capacity of the soil–pile system

Pile type	H_{crack}: N	M_{crack}: N m	H_u: N	M_{yield}: N m
Aluminium	—	—	695.1	82.8
Reinforced concrete	46.1	2.7	76.6	4.9

2689 kg/m^3. The coefficient of uniformity was determined as 2.97. The minimum and maximum dry densities were determined as 1505 and 1754 kg/m^3, respectively (ASTM D 4253-16 (ASTM, 2016a) and D 4254-16 (ASTM, 2016b)). During model preparation, the sand was pluviated from a constant height into the strongbox around the pre-installed pile to obtain a density of approximately 1700 kg/m^3, which corresponds to a relative density of approximately 80%. Based on oedometer test results at this relative density, a representative Young's modulus for the silica sand, as placed, was determined as 47 MPa, assuming a Poisson's ratio of approximately 0.3. The friction angle of the sand was obtained from triaxial tests as 32°.

From the measured properties of the pile and the soil, the ultimate horizontal pile capacity (H_u) of both piles were calculated as indicated in Table 4. This was based on methods and equations presented by Poulos and Davis (1980), originally proposed by Broms (1964), taking into account the properties of both the pile and the surrounding soil as indicated by Equations 1 and 2.

$$1. \quad H_u = \frac{0.5\,\gamma\,D_m\,L_m^3\,K_p}{e_L + L_m}$$

$$2. \quad M_{max} = H_u\left[e_L + \frac{2}{3}(0.82)\sqrt{\frac{H_u}{D_m\,K_p\gamma}}\right]$$

where γ is the unit weight of the soil, D_m is the outer diameter of the model pile, L_m is the embedment length of the model pile, K_p is the passive earth pressure coefficient, e_L is the load eccentricity from the soil surface and M_{max} is the maximum bending moment in the pile. Calculations predicted that the scaled aluminium and reinforced-concrete piles should yield. Thus, the maximum bending moment indicated in Table 4 corresponds to the yielding moment of the pile. For the yielding moment of the aluminium pile, the flexural stress equation ($M_{yield} = \sigma_{yield} I_m/(D_m/2)$) was used, assuming that the yield stress of the aluminium is 270 MPa (Gere and Goodno, 2013).

The capacity of the reinforced-concrete pile was established by plotting the flexural rigidity, $E_m I_m$, of the concrete section against the bending moment for different concrete conditions. These conditions include the uncracked, partially cracked (M_{crack}) and fully cracked (M_{yield}) sections, meeting the

requirements of strain compatibility and equilibrium of forces. Table 4 also includes the lateral load (H_{crack}) and corresponding bending moment (M_{crack}) required to cause cracking of the reinforced-concrete pile. Furthermore, although both scaled piles were supposed to model a full-scale 600 mm dia. reinforced-concrete pile, the use of aluminium for modelling full-scale reinforced-concrete piles should be questioned due to the ultimate bending capacity that is significantly larger than that typically expected for a reinforced-concrete pile.

A total of three tests were conducted at 30***g***. The first test was a monotonic lateral load test on the scaled aluminium pile, loading the pile to a load magnitude of 100 N. This test was followed by a second test where the pile was exposed to cyclic lateral loading to three different load magnitudes, applying these loads for a number of cycles (see Table 5). This allowed for comparison between the behaviour of the same pile under monotonic and cyclic conditions. The third test was conducted on a scaled reinforced-concrete pile, with the pile only loaded cyclically. Table 6 indicates the three different load magnitudes that the reinforced-concrete pile was subjected to, along with the corresponding number of load cycles.

The horizontal loads applied to the piles (as indicated in Tables 5 and 6) were limited to loads causing moments, respectively:

- smaller than the cracking moment of the reinforced-concrete pile
- between the cracking and yield moment of the reinforced-concrete pile – which would typically represent service conditions for reinforced concrete and
- exceeding the yielding moment of the reinforced concrete.

Based on the values presented in Table 4 regarding the ultimate bending capacity of both piles, a small applied load of 30 N only amounted to 4% of the ultimate capacity of the aluminium pile, in comparison to 40% of the ultimate capacity of the reinforced-concrete pile.

Table 5. Average horizontal load and number of load cycles – aluminium

Average horizontal force: N	Number of cycles, *N*
50	300
90	1000
110	1000

Table 6. Average horizontal load and number of load cycles – reinforced concrete

Average horizontal force: N	Number of cycles, *N*
30	150
65	1000
100	1000

The rate of data recording for the strain gauges was limited to 5 Hz. Sufficient data had to be acquired to plot full hysteresis loops, thus the rate of load application was limited to approximately 10 N/s.

3. Test results

3.1 Load–displacement response

Figures 3(a) and 3(b) indicate the load–displacement response of the scaled aluminium and reinforced-concrete piles. The piles were loaded successively applying the load magnitudes as

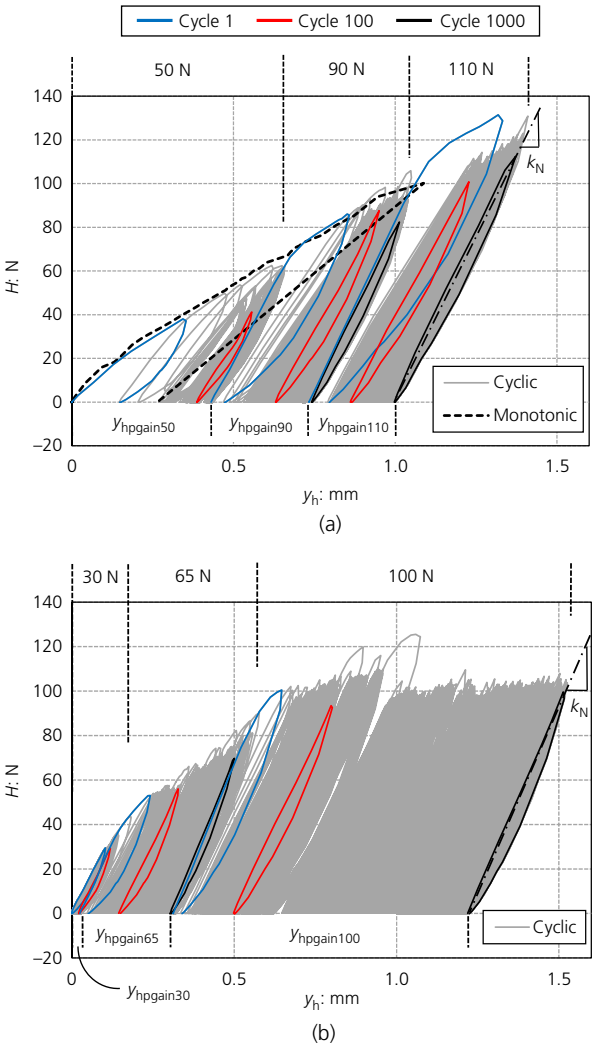

Figure 3. Load–displacement response: (a) aluminium; (b) reinforced concrete

presented in Tables 5 and 6, also indicated in Figures 3(a) and 3(b). Perfect load control was not possible. The load–displacement response for the monotonic test on the aluminium pile is also shown in Figure 3(a), indicated by a dashed line. In each part of Figure 3 cycle 1 (blue), cycle 100 (red) and cycle 1000 (black) are highlighted for the respective average load magnitudes, with the rest of the cycles shown in grey. In the case of the aluminium pile, it can be seen that the only difference between the load–displacement curves from the monotonic and cyclic tests was the permanent displacement experienced by the pile. The permanent displacement increased with load magnitude and number of load cycles.

The slope of the load–displacement curve for the monotonic test matched the static failure envelope from the cyclic lateral pile loading, illustrating that the maximum displacement of the pile was only affected by the magnitude of the applied load and not by the number of load cycles at a particular load.

The first load cycle at each load magnitude caused the most deformation of the surrounding soil, resulting in large hysteresis loops. After the first load cycle, the hysteresis loop width decreased with number of load cycles for both the aluminium and reinforced-concrete piles. For the aluminium pile, the load cycles became resilient after about ten cycles, which is similar to that observed by Werkmeister *et al.* (2001) within the plastic shakedown range (range A).

Considering the load–displacement response of the reinforced-concrete pile, behaviour similar to that observed by Lin and Liao (2006) for a pile with a changing flexural rigidity was seen. This was due to the concrete pile cracking, exhibiting non-linear behaviour as opposed to the aluminium pile, which behaved linearly. The reduction in flexural rigidity can be seen by the large permanent displacements that occurred during the load cycles at an applied load of 100 N. At low loads resilient behaviour was observed for the reinforced-concrete pile (Werkmeister *et al.*, 2001), with nearly no permanent displacement increase as the number of load cycles increased. However, as the applied load increased and the concrete cracked, increasing displacement occurred for each additional load application (range C) (Werkmeister *et al.*, 2001).

3.2 Bending moment response

The bending moment (M) development with depth below the soil surface (z_s) for the scaled aluminium and reinforced-concrete piles, respectively, under cyclic loading conditions, is presented in Figures 4(a) and 4(b). Depth $z_s = 0$ mm refers to the soil surface.

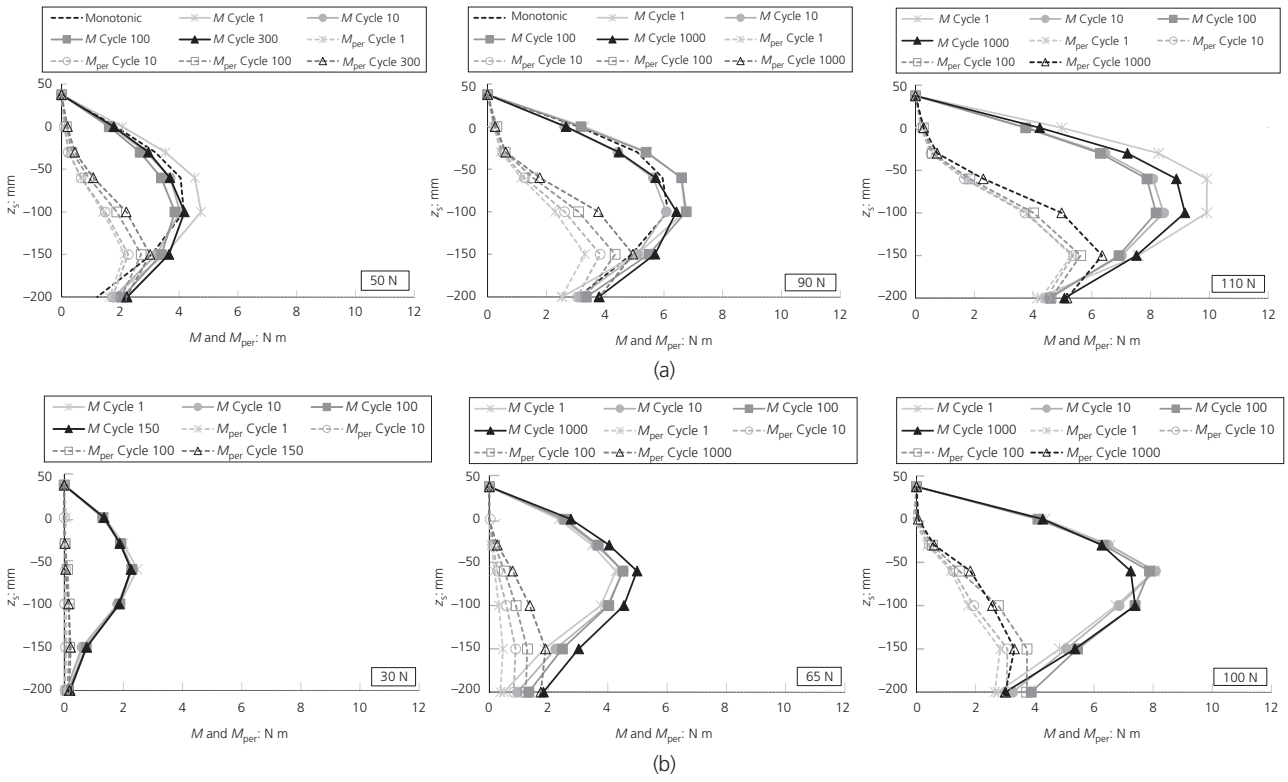

Figure 4. Bending moment response: (a) aluminium; (b) reinforced concrete

Load cycles 1, 10, 100 and 1000 at each load magnitude (H) are indicated, except for the aluminium pile at 50 N and reinforced-concrete pile at 30 N. Tests on the piles at these load magnitudes were only conducted to 300 cycles and 150 cycles, respectively, and are indicated as such along with cycle 1, cycle 10 and cycle 100. The bending moments for the reinforced-concrete pile incorporate the appropriate changes in the flexural rigidity after the pile section had cracked. For the aluminium pile, the results of the bending moments from the monotonic test are indicated with dashed lines. Figure 4 also indicates the permanent or locked-in moments (M_{per}) that remained in the aluminium and reinforced-concrete piles after load removal ($H = 0$ N) for the load cycles referred to above. As the magnitude of the applied load increased, the magnitude of the bending moment (M) and locked-in bending moment (M_{per}) increased in both piles.

No significant increase in the bending moment (M) was experienced by the aluminium pile, regardless of the number of load cycles. The maximum measured bending moment occurred approximately 100 mm (five pile diameters) below the soil surface and with the position of maximum bending moment unaffected by the number of load cycles. The locked-in bending moments also increased as the number of load cycles increased. These permanent moments were as a result of the changing soil conditions surrounding the pile, with permanent movement creating locked-in soil stresses in response to the applied cyclic lateral loads. The maximum permanent bending moment occurred approximately seven pile diameters (150 mm) below the soil surface, at a different location than the maximum bending moment (100 mm). Large differences between M and M_{per} existed towards the top of the pile, whereas the difference reduced at depths exceeding 100 mm, with M_{per} being about 50% of M at the same location under load application. At more than 200 mm below the soil surface differences between M_{per} and M were insignificant.

For the reinforced-concrete pile, the maximum measured bending moment occurred approximately three pile diameters below the soil surface (60 mm). The formation of the crack in the concrete section had minimal effect on the bending moment distribution in the pile, mainly due to the presence of steel reinforcement. Theoretically, the concrete section is predicted to crack at locations where the moment exceeds 2.7 N m (see Table 4), after which the elastic sectional properties of the pile no longer apply. Based on the observed strain data on both sides of the reinforced-concrete pile being fairly symmetrical (no cracking) at moments exceeding the cracking moment, elastic sectional properties were still applied to obtain the bending moments from these strains. Similar to the aluminium pile, M_{per} increased as the number of load cycles increased. The maximum permanent bending moment occurred approximately seven pile diameters below the soil surface (150 mm) as opposed to the 60 mm below the soil surface for the maximum bending moment. A slight reduction in the permanent bending moment with increasing number of load cycles seems to indicate crack growth. Large differences between M and M_{per} occurred, with M_{per} values of nearly 50% of M retained at 150 mm below the soil surface after load removal.

3.3 Accumulated lateral pile head displacement response

The effect of load magnitude and number of load cycles on the lateral displacement of the pile were considered. Figure 5 indicates the maximum lateral pile head displacement (y_h) and permanent pile head displacement (y_{hper}) against number of load cycles (N) for each load magnitude applied. The symbol y_h refers to the displacement as a result of the applied lateral load (H) and y_{hper} to the displacement remaining after the lateral load had been removed ($H = 0$ N). Figures 5(a)

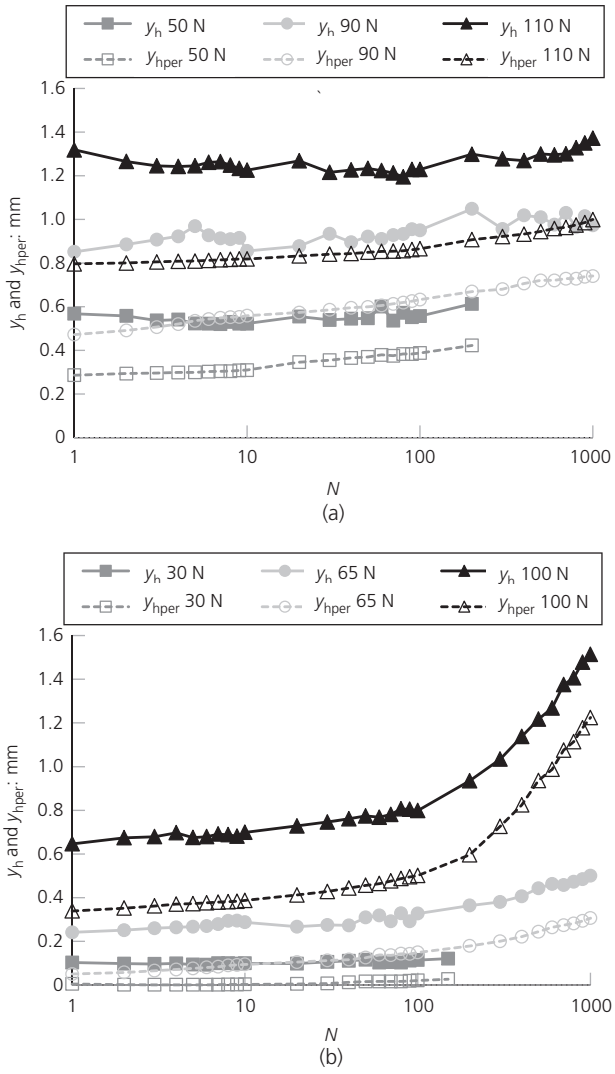

Figure 5. Pile head displacement: (a) aluminium; (b) reinforced concrete

and 5(b) present y_h and y_{hper} for the scaled aluminium and reinforced-concrete piles, respectively.

As the magnitude of the applied load and the number of load cycles increased, both y_h and y_{hper} increased, with the difference between them increasing as the load magnitude increased. As a result of densification of the sand caused by repetitive loading, the difference between y_h and y_{hper} reduced with number of load cycles. Permanent movement of the soil surrounding the piles occurred due to cyclic loading, resulting in permanent displacement of the pile, creating locked-in stresses in the soil and locked-in moments in the piles, similar to the observation by Li *et al.* (2010).

For the concrete pile no significant increase in y_h was observed under the 30 N load cycles. This was due to the reinforced-concrete section still being uncracked. However, the displacement of the pile head significantly increased after the formation of a crack as evident under an applied load of 100 N in Figure 5(b). As the crack propagated, the maximum and permanent displacements increased rapidly. The reinforced-concrete pile exhibited behaviour within the incremental plastic deformation range (range C proposed by Werkmeister *et al.* (2001)), with progressive plastic deformation and strains occurring for each load cycle at the same load level. This is in contrast to the behaviour of the aluminium pile, which exhibited behaviour within range A (plastic shakedown). Resilient behaviour of the soil was observed for the aluminium pile, with permanent displacement/strains gradually increasing with an increase in number of load cycles.

3.4 Secant pile stiffness response

The secant pile stiffness (see Figure 6) for both piles were determined to investigate the effect of load magnitude and number of load cycles. The secant pile stiffness for each pile was calculated using measured displacement of the pile under load application (see Figure 3). With both piles, for each load magnitude, the secant pile stiffness increased logarithmically with an increase in number of load cycles, which matched expectations from literature (Abadie and Byrne, 2014; Leblanc *et al.*, 2010; Li *et al.*, 2010; Little and Briaud, 1988). Densification is evident when considering the slopes of the logarithmic trendlines showing pile head displacement for the respective piles (see Figure 6). The rate at which the secant pile stiffness increased, decreases at higher load magnitudes. For the aluminium pile, a drastic increase in stiffness was observed under an applied load of 50 N between the first and second load cycles. This was due to the non-linear behaviour of the virgin soil. The secant pile stiffness increased slightly afterwards. This was not the case under applied loads of 90 and 110 N, even though non-linearity of the soil was still experienced (see Figure 3). The non-linearity of the loading curves over the first cycles at these loads were no longer evident due to the soil densification induced by previous load cycles. This was less evident in the case of the reinforced-concrete pile.

4. Discussion

To compare the cyclic load–displacement results of the two piles, static failure envelopes to the load–displacement responses were plotted. The difference in the flexural rigidity was accounted for by applying the relative stiffness ratio (EI_C/EI_A) of 1.63 to the displacement results of the reinforced-concrete pile. The relative stiffness ratio was obtained from the pile calibration exercise.

The load–displacement envelopes for both the scaled aluminium and reinforced-concrete piles are presented in Figure 7. From the start of the curve, even for an uncracked concrete section, the reinforced-concrete pile showed a stiffer response, exhibiting non-linear behaviour in comparison to the

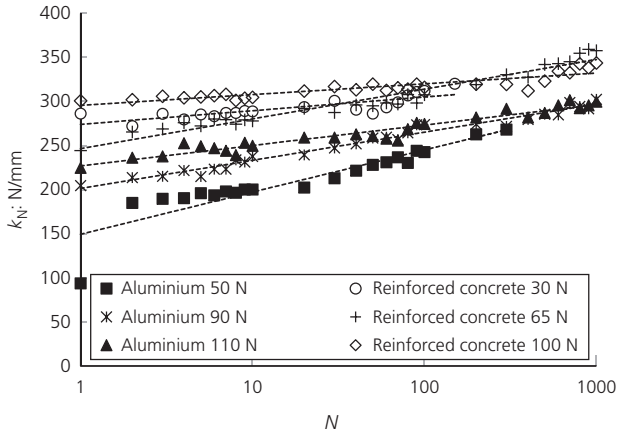

Figure 6. Combined secant pile stiffnesses

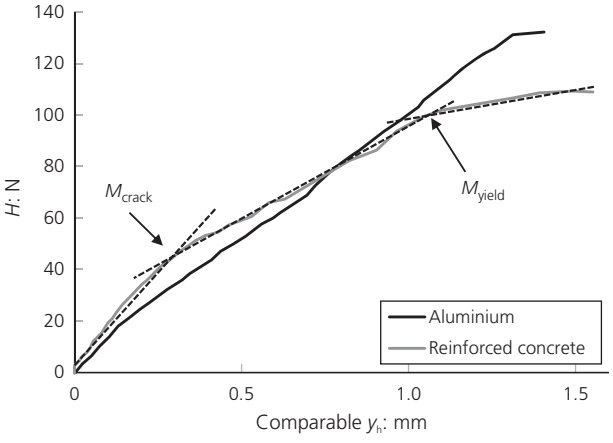

Figure 7. Static failure envelope

aluminium pile that showed a fairly linear response. The non-linear response of the concrete was further influenced by the formation of cracks in the section, resulting in a change in the stiffness of the pile at an applied load of approximately 50 N, which corresponds to the predicted cracking load (H_{crack}) of 46.1 N. The reinforced-concrete pile yielded at a load of about 95 N, which is slightly higher than the predicted value of 76.6 N. Large differences between the two piles occurred past the point of yielding largely due to the formation and propagation of cracks in the reinforced-concrete pile.

To investigate and compare the response of the soil to cyclic loading, both the secant pile stiffness of the soil–pile system and how it was influenced by not only the load magnitude but also the number of load cycles, were considered. Cycle 1000 for two load magnitudes are plotted in Figures 8(a) and 8(b) for the aluminium and reinforced-concrete piles, respectively. The slope of the secant pile stiffness (the line connecting the peak of the loading curve and the origin), converged to a constant value for each pile as the number of cycles increased. The secant pile stiffness (slope of the line) for the aluminium pile was calculated as 300 N/mm, where the slope for the reinforced-concrete pile was slightly steeper, calculated as 350 N/mm. Thus, based on this observation it appears that, regardless of the magnitude of the load, the secant pile stiffness converged to a constant value after a certain number of load cycles. This is similar to observations by Li *et al.* (2010). The formation of cracks did not influence the secant stiffness response, and it seems that the secant pile stiffness was mainly affected by the resilient modulus of the soil at the load magnitude applied.

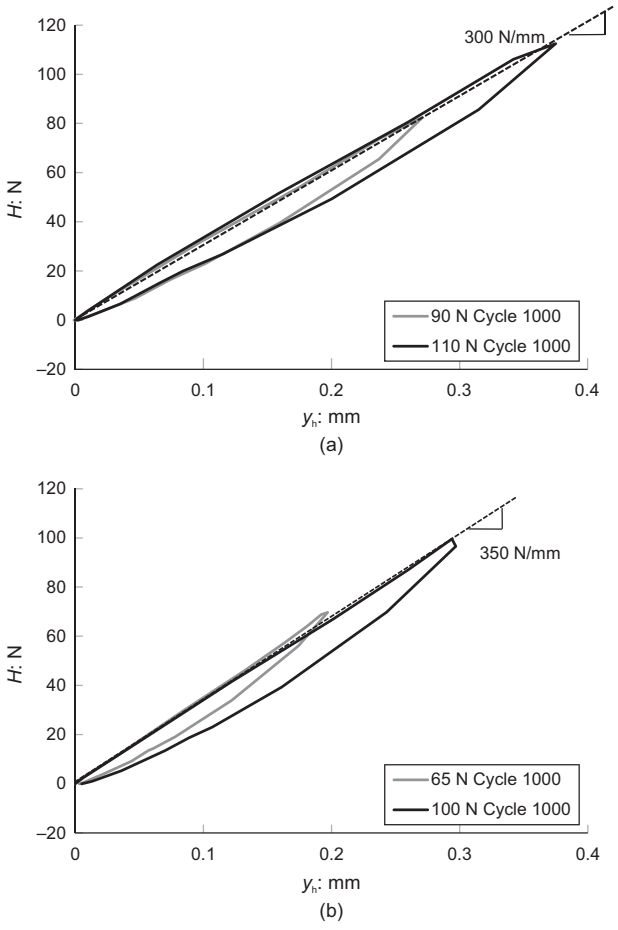

Figure 8. Secant stiffness cycles: (a) aluminium; (b) reinforced concrete

The permanent pile head displacement gain (y_{hpgain}) was calculated for each pile from the pile head displacement data, as indicated on the x-axis in both figures (Figures 3(a) and 3(b)). The symbol y_{hpgain} refers to the difference between the permanent displacement after the last load cycle and the permanent displacement at the start of the first load cycles for each applied load magnitude. The permanent pile displacement is largely influenced by the magnitude of the applied load and the number of load cycles. Therefore, even though the cyclic tests on the aluminium and reinforced-concrete piles were not conducted at the same load magnitudes and number of load cycles, a trend can be observed. The solid markers in Figure 9 present the permanent pile head displacement gain (y_{hpgain}) against the magnitude of the applied load for both piles after 1000 cycles at each load. The permanent pile head displacement gain for 50 N load on the aluminium pile and 30 N load on the reinforced-concrete pile are shown as unshaded markers to highlight that only 300 and 150 load cycles were, respectively, applied to the aluminium and reinforced-concrete piles at those loads.

For the aluminium pile, the permanent pile head displacement gain (y_{hpgain}) decreased as the magnitude of the applied load

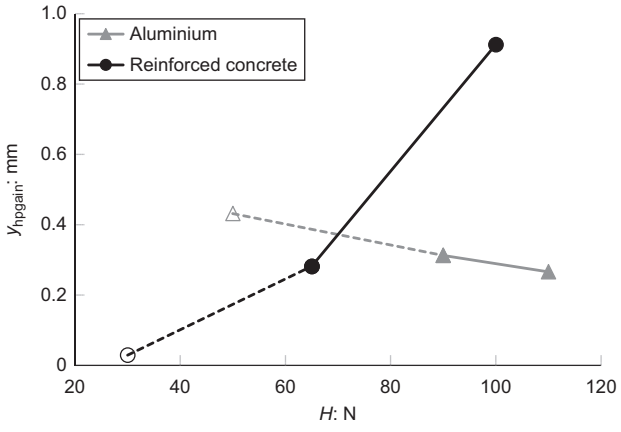

Figure 9. Permanent pile head displacement gain (comparison)

increased. This differs substantially from the behaviour of the reinforced-concrete pile, where y_{hpgain} increased with an increase in the load magnitude, even at low loads at which the reinforced-concrete pile had not yet yielded.

These trends indicate that for loads up to 110 N the aluminium pile behaviour was resilient, defined by the Werkmeister *et al.* (2001) range A, while the reinforced-concrete pile showed signs of incremental plastic deformation, or range C behaviour at loads below 100 N. The rate of increase in permanent pile head displacement for the reinforced-concrete pile was higher than the rate of decrease for the aluminium pile even at relatively small loads. This can be explained by the continued formation and gradual propagation of cracks in the concrete section with increasing load cycles, resulting in a steep increase in the permanent pile head displacement after 65 N. This behaviour confirms the observations by Little and Briaud (1988) that a change in flexural pile stiffness (cracking) cause greater degradation to the soil–pile system.

5. Conclusions

Significant differences between the behaviour of the reinforced-concrete and aluminium piles were observed when subjected to horizontal cyclic loading, even at low applied cyclic loads. Considering the static failure envelope of both piles, the response of the reinforced-concrete pile was non-linear from the start of load application, in contrast to the fairly linear initial response of the aluminium pile. The non-linear behaviour of the reinforced-concrete pile was influenced by cracking and yielding that occurred in the pile as the number of load cycles and the magnitude of the applied load increased.

The overall load–displacement response of both pile types to cyclic loading indicated densification of the soil in front of the pile with an increase in the number of load cycles. The secant pile stiffness converged to a constant value, regardless of the magnitude of the applied load and the number of load cycles. The formation of cracks did not seem to have an influence on the secant pile stiffness response, indicating that the secant pile stiffness is possibly only a function of soil stiffness, with the effect of pile stiffness being limited.

Significant permanent displacement was observed for the reinforced-concrete pile after the formation of cracks in the section. This cannot occur in aluminium piles. The permanent displacement associated with a given number of load cycles increased for the reinforced-concrete pile and stabilised for the aluminium pile as the magnitude of the applied load increased (given the load ranges considered).

Therefore, based on the observed results, fundamental differences can be expected in the behaviour of reinforced-concrete and aluminium model piles subjected to horizontal loading. Differences in behaviour were evident at loads even smaller than those predicted to cause cracking.

It is concluded that the behaviour of reinforced-concrete elements subjected to loads causing cracking will not be captured using materials that cannot replicate the reduction in stiffness resulting from crack formation in concrete at serviceability loads.

Acknowledgements

The financial support of the Concrete Institute and the Concrete Society of Southern Africa is gratefully acknowledged.

REFERENCES

Abadie CN and Byrne BW (2014) Cyclic loading response of monopile foundations in cohesionless soils. In *Proceedings of the 8th International Conference on Physical Modelling in Geotechnics* (Gaudin C and White D (eds)). Taylor & Francis Group, London, UK, vol. 2, pp. 779–784.

ASTM (2016a) D 4253-16: Standard test methods for maximum index density and unit weight of soils using vibratory table. ASTM International, West Conshohocken, PA, USA.

ASTM (2016b) D 4254-16: Standard test methods for minimum index density and unit weight of soils and calculation of relative density. ASTM International, West Conshohocken, PA, USA.

Broms BB (1964) Lateral resistance of piles in cohesionless soils. *Proceedings of the American Society of Civil Engineers – Journal of Soil Mechanics and Foundation Engineering* **90(3)**: 123–156.

Brown DA, Reese LC and O'Neill MW (1987) Cyclic lateral loading of a large-scale pile group. *Journal of Geotechnical Engineering* **113(11)**: 1326–1343.

Byrne G and Berry AD (2008) *A Guide to Practical Geotechnical Engineering in Southern Africa*. Franki, Johannesburg, South Africa.

Dyson GJ and Randolph MF (2001) Monotonic lateral loading of piles in calcareous sand. *Journal of Geotechnical and Geoenvironmental Engineering* **127(4)**: 346–352.

Georgiadis M, Anagnostopoulos C and Saflekou S (1992) Centrifugal testing of laterally loaded piles in sand. *Canadian Geotechnical Journal* **29(2)**: 208–216.

Gere JM and Goodno BJ (2013) *Mechanics of Materials*. Cengage Learning, Stamford, CT, USA.

Jacobsz SW, Kearsley EP and Kock JHL (2014) The geotechnical centrifuge facility at the University of Pretoria. In *Proceedings of the 8th International Conference on Physical Modelling in Geotechnics* (Gaudin C and White D (eds)). Taylor & Francis Group, London, UK, vol. 1, pp. 169–174.

Johnson KL (1986) Plastic flow, residual stresses and shakedown in rolling contacts. *Proceedings of the 2nd International Conference on Contact Mechanics and Wear of Rail/Wheel Systems* (Gladwell GML, Ghonem H and Kalousek J). University of Waterloo Press, Waterloo, ON, Canada, pp. 83–97.

Kirkwood PB and Haigh SK (2014) Centrifuge testing of monopiles subject to cyclic lateral loading. In *Proceedings of the 8th International Conference on Physical Modelling in Geotechnics*

(Gaudin C and White D (eds)). Taylor & Francis Group, London, UK, vol. 2, pp. 827–831.

Leblanc C, Houlsby GT and Byrne BW (2010) Response of stiff piles in sand to long-term cyclic lateral loading. *Géotechnique* **60(2)**: 79–90, https://doi.org/10.1680/geot.7.00196.

Li Z, Haigh SK and Bolton MD (2010) Centrifuge modelling of mono-pile under cyclic lateral loads. In *Proceedings of the 7th International Conference on Physical Modelling in Geotechnics* (Springman S, Laue J and Seward L (eds)). CRC Press, London, UK, pp. 965–970.

Li W, Igoe D and Gavin K (2015) Field test to investigate the cyclic response of monopiles in sand. *Proceedings of the Institution of Civil Engineers – Geotechnical Engineering* **168(GE5)**: 407–421, https://doi.org/10.1680/jgeen.14.00104.

Li W, Zhu B and Yang M (2017) Static response of monopile to lateral load in over-consolidated dense sand. *Journal of Geotechnical and Geoenvironmental Engineering* **143(7)**: 04017026.

Lin SS and Liao JC (2006) Lateral response evaluation of single piles using inclinometer data. *Journal of Geotechnical and Geoenvironmental Engineering* **132(12)**: 1566–1573.

Lin H, Ni L, Suleiman MT and Raich A (2015) Interaction between laterally loaded pile and surrounding soil. *Journal of Geotechnical and Geoenvironmental Engineering* **141(4)**: 04014119.

Little RL and Briaud JL (1988) *Full Scale Cyclic Lateral Load Tests on Six Single Piles in Sand*. Geotechnical Division, Department of Civil Engineering, Texas A and M University, College Station, TX, USA, Miscellaneous Paper GL-88-27.

Long JH and Vanneste G (1994) Effects of cyclic lateral loads on piles in sand. *Journal of Geotechnical Engineering* **120(1)**: 225–244.

Madabhushi G (2015) *Centrifuge Modelling for Civil Engineers*. CRC Press, Boca Raton, FL, USA.

Mosley B, Bungey J and Hulse R (2012) *Reinforced Concrete Design to Eurocode 2*. Palgrave Macmillan, London, UK.

Nip DCN and Ng CWW (2005) Back-analysis of laterally loaded bored piles. *Proceedings of the Institution of Civil Engineers – Geotechnical Engineering* **158(2)**: 63–73, https://doi.org/10.1680/geng.2005.158.2.63.

Noor FA and Boswell LF (1992) *Small Scale Modelling of Concrete Structures*. Elsevier Applied Science, London, UK.

Poulos HG and Davis EH (1980) *Pile Foundation Analysis and Design*. John Wiley & Sons, Toronto, Canada.

Poulos HG and Hull T (1989) The role of analytical geomechanics in foundation engineering. In *Foundation Engineering: Current Principles and Practices* (Kulhawy FH (ed.)). ASCE, Reston, VA, USA, pp. 1578–1606.

Reese LC, Cox WR and Koop FD (1974) Analysis of laterally loaded piles in sand. In *Offshore Technology in Civil Engineering: Hall of Fame Papers from the Early Years* (Templeton JS (ed.)). ASCE, Reston, VA, USA, paper no. 2080, pp. 473–483.

Ruesta PF and Townsend FC (1997) Evaluation of laterally loaded pile group at Roosevelt Bridge. *Journal of Geotechnical and Geoenvironmental Engineering* **123(12)**: 1153–1161.

Sabnis GM, Harris HG, White RN and Saeed Mirza M (1983) *Structural Modeling and Experimental Techniques*. Prentice-Hall, Englewood Cliffs, NJ, USA.

Schofield AH (1980) Cambridge geotechnical centrifuge operations. *Géotechnique* **30(3)**: 227–268, https://doi.org/10.1680/geot.1980.30.3.227.

Taylor RN (1995) *Geotechnical Centrifuge Technology*. Blackie Academic & Professional, Glasgow, UK.

Verdure L, Garnier J and Levacher D (2003) Lateral cyclic loading of single piles in sand. *International Journal of Physical Modelling in Geotechnics* **3(3)**: 17–28, https://doi.org/10.1680/ijpmg.2003.030303.

Werkmeister S, Dawson AR and Wellner F (2001) Permanent deformation behaviour of unbound granular materials and the shakedown theory. *Transportation Research Record* **1757**: 75–81.

Yan L and Byrne PM (1992) Lateral pile response to monotonic pile head loading. *Canadian Geotechnical Journal* **29(6)**: 955–970.

Zhu B, Li T, Xiong G and Lui JC (2016) Centrifuge model tests on laterally loaded piles in sand. *International Journal of Physical Modelling in Geotechnics* **16(4)**: 160–172, https://doi.org/10.1680/jphmg.15.00023.